



**HAL**  
open science

## Tuning the Mn<sub>5</sub>Ge<sub>3</sub> and Mn<sub>11</sub>Ge<sub>8</sub> thin films phase formation on Ge(111) via growth process

Mohamed-Amine Guerboukha, Matthieu Petit, Aurélie Spiesser, Alain Portavoce, Omar Abbes, Vasile Heresanu, Sylvain Bertaina, Cyril Coudreau,  
Lisa Michez

► **To cite this version:**

Mohamed-Amine Guerboukha, Matthieu Petit, Aurélie Spiesser, Alain Portavoce, Omar Abbes, et al.. Tuning the Mn<sub>5</sub>Ge<sub>3</sub> and Mn<sub>11</sub>Ge<sub>8</sub> thin films phase formation on Ge(111) via growth process. Thin Solid Films, 2022, 761, pp.139523. 10.1016/j.tsf.2022.139523 . hal-04272525

**HAL Id: hal-04272525**

**<https://hal.science/hal-04272525v1>**

Submitted on 7 Nov 2023

**HAL** is a multi-disciplinary open access archive for the deposit and dissemination of scientific research documents, whether they are published or not. The documents may come from teaching and research institutions in France or abroad, or from public or private research centers.

L'archive ouverte pluridisciplinaire **HAL**, est destinée au dépôt et à la diffusion de documents scientifiques de niveau recherche, publiés ou non, émanant des établissements d'enseignement et de recherche français ou étrangers, des laboratoires publics ou privés.

# Tuning the $\text{Mn}_5\text{Ge}_3$ and $\text{Mn}_{11}\text{Ge}_8$ thin films phase formation on Ge(111) via growth process

5 Mohamed-Amine Guerboukha<sup>1</sup>, Matthieu Petit<sup>1</sup>, Aurélie Spiesser<sup>2</sup>, Alain Portavoce<sup>3</sup>, Omar Abbas<sup>3</sup>,  
Vasile Heresanu<sup>1</sup>, Sylvain Bertaina<sup>3</sup>, Cyril Coudreau<sup>1</sup>, Lisa Michez<sup>1</sup>

<sup>1</sup> Aix Marseille Univ, CNRS, CINaM, Marseille, France

10 <sup>2</sup> Research Center for Emerging Computing Technologies, Natl Inst Adv Ind Sci & Technol (AIST),  
1-1-1 Umezono, Tsukuba, Ibaraki 3058568, Japan

<sup>3</sup> Aix Marseille Univ, CNRS, IM2NP, Marseille, France

## 15 **corresponding author:**

Matthieu Petit

address: CINaM-CNRS, campus de Luminy, Case 913, 13288 Marseille Cedex 9, France

phone number: +33 6 62 92 28 65

E-mail address: [matthieu.petit@univ-amu.fr](mailto:matthieu.petit@univ-amu.fr)

20

## **keywords:**

Thin film; Germanide; Phase formation; epitaxy; Molecular beam epitaxy;  $\text{Mn}_5\text{Ge}_3$ ;  $\text{Mn}_{11}\text{Ge}_8$

## 25 **Abstract**

We have studied the stability of manganese germanide thin films grown on Ge(111) substrates by three different growth methods: solid phase epitaxy, reactive deposition epitaxy and co-deposition. By combining X-ray diffraction and magnetic measurements, we demonstrate that we can form either  $\text{Mn}_5\text{Ge}_3$  or  $\text{Mn}_{11}\text{Ge}_8$  thin films depending on the growth processes. In the case of solid phase epitaxy, we explain the phase formation sequence by taking into consideration the kinetic and thermodynamic processes involved. Tuning phase formation of the manganese germanide thin films was determined using in situ X-ray diffraction and the effect of the thin film thickness on the  $\text{Mn}_5\text{Ge}_3$  thermal stability was investigated.

30

## 1. Introduction

35 Magnetic thin films are extensively used in data storage, magnetic sensors, and other spintronics technologies [1]. To achieve the desired magnetic properties, a precise control of phase formation during thin film growth is usually required. The driving forces that govern phase formation include several factors such as nucleation barrier, interface energy and diffusion flux [2,3]. Also phases generally appear sequentially and not simultaneously, and also strongly depend on the film  
40 thickness [4]. Thus, understanding the mechanisms of phase formation as a function of the film thickness is an important advantage for device applications.

The interest in the manganese germanide compounds mainly stems from the  $Mn_5Ge_3$  alloy which exhibits interesting features for spintronic applications. This ferromagnetic compound has a Curie temperature ( $T_C$ ) of 296 K that can be increased by carbon insertion up to 450 K. Its hexagonal  $D8_8$ -  
45 type crystal structure ( $a_{hex} = 7.18 \text{ \AA}$ ,  $c_{hex} = 5.05 \text{ \AA}$ , prototype structure  $Mn_5Si_3$ ) enables the epitaxial growth of thin films on Ge(111) substrates with the following relationships:  $Mn_5Ge_3(0001)//Ge(111)$  and  $Mn_5Ge_3[1-100]//Ge[11-2]$  with a lattice mismatch of -3.75% [5–8]. Studies about the magnetic and electrical properties and the several growth methods of  $Mn_5Ge_3$  thin films on Ge(111) substrates have demonstrated the assets of this intermetallic alloy as a ferromagnetic electrode for spin  
50 injection for instance [9–13]. Moreover  $Mn_{11}Ge_8$ , sometimes referred as  $Mn_3Ge_2$ , is another manganese germanide phase exhibiting interesting magnetic properties.  $Mn_{11}Ge_8$  is a non-collinear antiferromagnet below 150 K and a ferromagnet up to 274 K [14]. Its orthorhombic crystal structure is closed to the  $Mn_5Ge_3$  structure with  $a = 13.21 \text{ \AA}$ ,  $b = 15.88 \text{ \AA}$ ,  $c = 5.09 \text{ \AA}$  (prototype structure  $Cr_{11}Ge_8$ ). Theoretical predictions suggest the possibility of epitaxial growth on Ge(111) [15].

55 The present work combines X-ray diffraction (XRD) and magnetic measurements to study the formation and stability of epitaxial  $Mn_5Ge_3$  and  $Mn_{11}Ge_8$  thin films on Ge(111) substrates via different growth methods: solid phase epitaxy (SPE), reactive deposition epitaxy (RDE) or co-deposition epitaxy. Emphasis is given on the SPE process to determine the formation sequence of germanide phases and the stability of the  $Mn_5Ge_3$  films as a function of the film thickness.

60

## 2. Growth methods and experimental details

Thin epitaxial films of  $Mn_5Ge_3$  and  $Mn_{11}Ge_8$  were grown on high-purity Ge(111) substrates in a molecular beam epitaxy chamber with a base pressure better than  $2 \times 10^{-7}$  Pa. To obtain a flat, smooth, and oxide-free surface, we cleaned the Ge substrates following this method: first, the  
65 samples were immersed in an acetone solution and sonicated for 10 minutes, then immersed in an isopropanol alcohol ultrasonic bath for another 10 minutes in order to degrease the surface and finally immersed in a last bath containing a 50% HF acid - 50%  $H_2O$  mixture to remove the native oxide. Subsequently, we performed *in situ* thermal annealing for several minutes at 720 K followed

by flash annealing at 1020 K to remove the residual Ge surface oxide, which can be formed during sample transfer into high vacuum. Eventually a 50 nm thick Ge buffer is deposited to bury any remaining surface impurities and to ensure that the starting surface before the deposition is perfectly cleaned. In this present article, the films were grown using three techniques, schematized on fig.1.

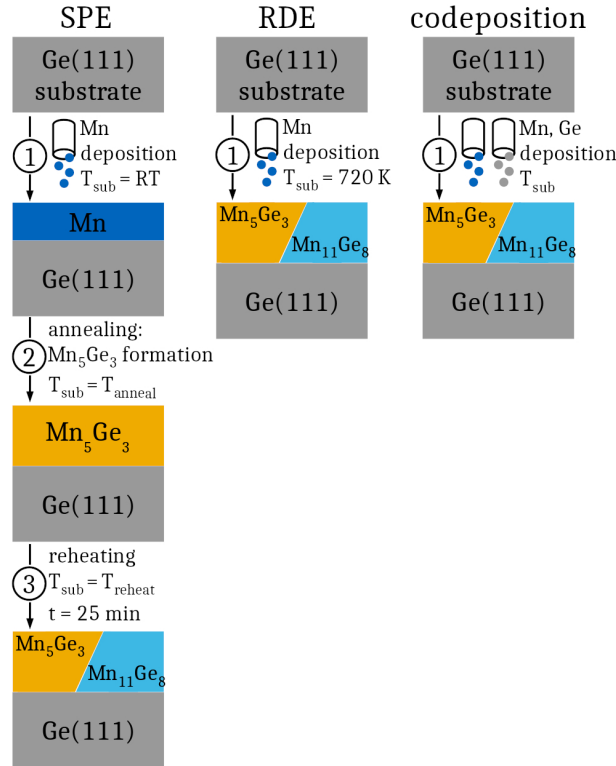


**Figure 1: Three different growth methods were used to form the  $\text{Mn}_5\text{Ge}_3$  or  $\text{Mn}_{11}\text{Ge}_8$  thin films on Ge(111) substrates: the solid phase epitaxy (SPE), the reactive deposition epitaxy (RDE) and the co-deposition of Mn and Ge atoms.**

The first technique is the SPE technique used to synthesize the first  $\text{Mn}_5\text{Ge}_3$  thin films on a Ge(111) substrate. It consists in the deposition of a Mn layer at room temperature (RT) onto the Ge(111) substrate, followed by a thermal anneal at a temperature around 720 K to activate the interdiffusion of Mn and Ge atoms and the nucleation of the phases. The second method is the RDE: the substrate is heated up to 720 K and kept at this temperature during the deposition of Mn. The third growth technique is the co-deposition of Mn and Ge with the 5:3 stoichiometric flux and at a given substrate temperature. The last two growth methods enable the controlled nucleation of the phase formation [16]. The chamber is fitted out with a reflection high-energy electron diffraction (RHEED) system to monitor and check *in situ* these growth processes. Mn and Ge atoms are evaporated from Knudsen cell. The flux are carefully calibrated using a quartz crystal microbalance and RHEED oscillations. Structural characterizations were carried out by XRD. XRD patterns were collected using a rotating anode Rigaku RU200BH (non-monochromatic  $\text{CuK}\alpha 1$  radiation  $\lambda=1.541\text{\AA}$ ) equipped with a 2D Mar345 detector. Data were collected over a  $2\theta$  range of 20-65°.

The XRD curves ( $2\theta$  versus intensity) are drawn by integrating the intensity of the 2D XRD maps. Magnetic characterizations of the grown films were performed using a superconducting quantum interference device magnetometer Quantum Design MPMSXL in a temperature range varying from 5 to 350 K. The temperature dependence of the magnetization has been recorded using a constant 0.1 T external in-plane magnetic field.

### 3. $\text{Mn}_5\text{Ge}_3$ and $\text{Mn}_{11}\text{Ge}_8$ heats of formation

Phase formation has been widely studied in the case of thin films growth taking into account equilibrium, diffusion processes as well as interface and stress energy [17–22]. According to the bulk Ge-Mn phase diagram,  $\text{Mn}_{11}\text{Ge}_8$  is the Ge richer -non-congruent- phase which undergoes a peritectic transition into  $\text{Mn}_5\text{Ge}_3$  and liquid around 1042 K.  $\text{Mn}_5\text{Ge}_3$  is a congruent phase melting at  $\sim 1245$  K and the closest one to the lowest eutectic (993 K, Ge concentration = 57%at) [23]. This lowest eutectic is also the eutectic closest to the center of the Mn-Ge diagram.

The effective heat of formation (EHF) model is a useful tool to explain the phase formed according to the growth techniques [24–26]. It was initially developed to predict the sequence of the phase formation during film growth in the case of a solid phase interaction. The driving force of a reaction is the decrease of the Gibbs free energy ( $\Delta G = \Delta H - T\Delta S$ , T the temperature,  $\Delta H$  and  $\Delta S$  the enthalpy and entropy variations respectively). As we considered only solid-state reaction,  $\Delta S$  is negligible, thus  $\Delta H$  is a relevant approximation for the variation of  $\Delta G$ . However, the local concentrations of atoms at the interface where the reaction occurs must be taken into account since it represents the real amount of atoms locally available for the reaction. These local concentrations depend on the different atoms flux caused by the diffusion phenomena and by the evaporation flux from the effusion cells. The expression of the effective heat of formation  $\Delta H'$  can be found in ref. [24]. The heat of formation  $\Delta H^0$  of the two germanide intermetallic compounds are close: Berche et al. proposed  $\Delta H^0 = -17.5 \pm 0.3 \text{ kJ} \cdot (\text{mol} \cdot \text{at})^{-1}$  for  $\text{Mn}_{11}\text{Ge}_8$  and  $\Delta H^0 = -18.4 \pm 0.3 \text{ kJ} \cdot (\text{mol} \cdot \text{at})^{-1}$  for  $\text{Mn}_5\text{Ge}_3$  [27]. Injecting these values into the effective heat of formation (EHF) model, we can draw the triangular diagram (cf. Fig.2) representing the effective heats of formation  $\Delta H'$  of  $\text{Mn}_5\text{Ge}_3$  and  $\text{Mn}_{11}\text{Ge}_8$  as a function of the Mn concentration.

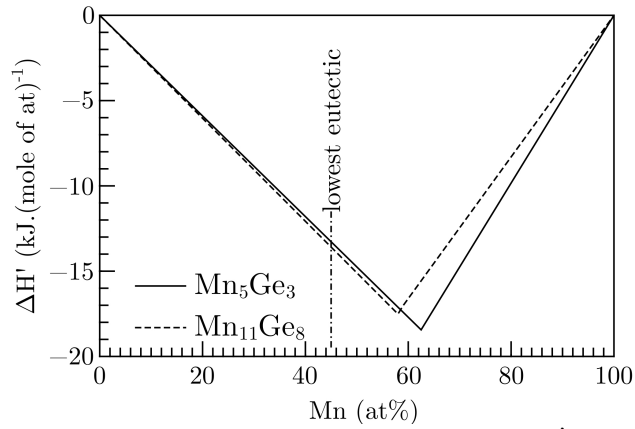


**Figure 2: The effective heats of formation  $\Delta H'$  of the phases  $Mn_5Ge_3$  and  $Mn_{11}Ge_8$  versus the Mn concentration.**

If the relative concentration of Mn is higher than 58.5at, the formation of the  $Mn_5Ge_3$  phase is more favorable than the  $Mn_{11}Ge_8$  one, germanium being the limiting element in the phase formation. These results are consistent with the first principle study on the Mn-Ge systems made by Arras et al. [15]. At the growth interface, the local concentrations of Mn and Ge atoms can be changed according to the flux of diffusion of both species or according to the deposition flux, thus moving the equilibrium. However, the EHF model does not take into account the nucleation barrier of the phases nor the interface energy. These aspects depend on the congruency or non-congruency of the phases near the lowest eutectic. Usually, a low eutectic means low interfacial energy and low nucleation barrier. The Walser-Bené (W-B) rule enriched by Ronay and Bené deals with these considerations. It was established to predict the first nucleated phase and the subsequent one at planar interfaces [17,22,28]. Merging the W-B rule and the EHF model, the first phase to form at a planar metal-germanium interface in a solid state reaction should be the congruent phase neighboring the eutectic closest to the center of the phase diagram (in at%) and with the lowest effective heat of formation. This phase is  $Mn_5Ge_3$  in the case of a Mn thin film on a Ge substrate according to the binary Mn-Ge phase diagram.

## 4. Results and discussion

### 4.1 Growth modes and phase formation

For each growth modes, the initial surfaces consist of the Ge buffer layer ones. These surfaces are 2D and are checked by RHEED prior to any further growth processes. The *in situ* RHEED monitoring of thin films synthesized according to the different growth methods show that the corresponding films surfaces remain 2D.

$Mn_5Ge_3$  thin films were historically first synthesized using the technique of the SPE [5]. For 70 nm thick films and an annealing temperature of 720 K, this technique produces mono-crystalline thin

140 films where only the  $Mn_5Ge_3$  phase is detected either using XRD measurements (fig.3 a) and g)) or magnetization versus temperature ( $M(T)$ ) technique (fig.3 d)). The image of Fig3.g) is a typical 2D-XRD map recording with the Mar345 2D detector and is consistent with a single crystal  $Mn_5Ge_3$  layer with the c-axis normal to the sample surface, the position of the diffraction spots being in good agreement with the reflections (as indicated on the map) mentioned in the reference card of  $Mn_5Ge_3$  (ICSD-01-089-4887). Especially the peak at  $2\theta = 35.48^\circ$  is attributed to the  $Mn_5Ge_3(002)$  plans. The  $M(T)$  curve gradually decreases to reach almost after 299 K which is typical of a ferromagnetic material with a  $T_C = 299$  K.

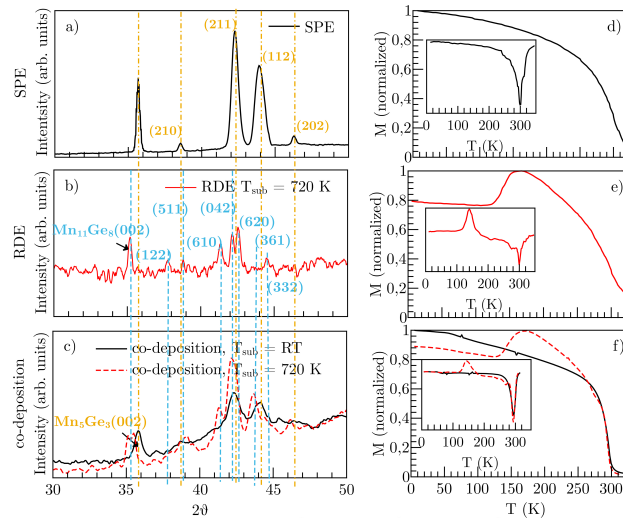


**Figure 3:** a-c) X-ray diffraction measurements of manganese germanide thin films grown on Ge(111) substrates according to the three growth methods: SPE, RDE and co-deposition from top to bottom. Yellow dashed and dots lines index the  $Mn_5Ge_3$  related peaks, the cyan dashed line index the  $Mn_{11}Ge_8$  peaks. g) 2D-XRD map of a  $Mn_5Ge_3$  film grown by SPE. The black indexes correspond to the Ge(111) substrate, the yellow ones to the  $Mn_5Ge_3$  film. d-f) Normalized magnetizations versus temperature for the  $Mn_5Ge_3$  thin films according to the used growth methods. The insets display the corresponding derivative curves  $dM/dT$ . The inflection points of the  $M(T)$  curves are deduced from the minima of the curves, and corresponds to the Curie temperatures.

On the contrary, in the case of the RDE growth mode, XRD shows the predominantly existence of the  $Mn_{11}Ge_8$  phase with the (002) peak at  $2\theta = 35.40^\circ$ .  $M(T)$  analysis displays an antiferromagnetic transition at 145 K and two ferromagnetic transitions at 270 and 293 K, attributed to the co-existence of the  $Mn_5Ge_3$  and  $Mn_{11}Ge_8$  compound in the thin film. As for the SPE synthesis, the W-B rule prevails at the interface between the Ge substrate and the Mn metallic film:  $Mn_5Ge_3$  nucleates first, being the closest congruent phase to the eutectic in the Mn-Ge binary diagram. The RDE involves two concomitant phenomena, the interdiffusion between the Ge atoms of the substrate and the atoms of the Mn film as well as the phase nucleation. The Mn flux emitted by the Knudsen cell

being rather low ( $\sim 0.3 \text{ nm.s}^{-1}$ ), every Mn atoms reaching the sample surface is immediately consumed: the nucleation of the phase with the lowest Mn concentration is favored, leading to the formation of  $\text{Mn}_{11}\text{Ge}_8$  as predicted by the values of the effective enthalpy of formation. The deposition rate which determines the supply of Mn atoms control the selection of the formed phase. The detection of the  $\text{Mn}_5\text{Ge}_3$  phase is explained by the concept of the critical thickness of the first forming phase before a second phase could start growing [29–31]. As the deposition time increases, the thickness of the  $\text{Mn}_{11}\text{Ge}_8$  thin film also increases. The Ge atoms coming from the substrate then diffuse through this film which slows down the Ge supply at the now  $\text{Mn}_{11}\text{Ge}_8$  surface. The local relative concentration shifts toward Mn richer environment, favoring the nucleation of  $\text{Mn}_5\text{Ge}_3$  according to fig.2.

Regarding the co-deposition, two thin films were synthesized using two different substrate temperatures: RT and 720 K. In the case of  $T_{\text{sub}} = \text{RT}$ , XRD and  $M(T)$  measurements only reveal the presence of the  $\text{Mn}_5\text{Ge}_3$  phase as a mono-crystalline thin film. The accurate control of the stoichiometric ratio of the Mn and Ge fluxes combined with the low interface energy ( $\gamma_{\text{Mn}_5\text{Ge}_3/\text{Ge}(111)} = 0.53 \text{ J.m}^{-2}$ ) of the  $\text{Mn}_5\text{Ge}_3/\text{Ge}(111)$  system promote the  $\text{Mn}_5\text{Ge}_3$  phase formation [15,28,32]. At  $T_{\text{sub}} = 720 \text{ K}$ , the  $\text{Mn}_{11}\text{Ge}_8$  phase is detected and the thin film is polycrystalline. The peak around  $2\theta = 35^\circ$  exhibits two contributions attributed to the (002) plans of  $\text{Mn}_5\text{Ge}_3$  and  $\text{Mn}_{11}\text{Ge}_8$ . Like the RDE experiments, the  $M(T)$  curve shows the antiferromagnetic transition around 150 K and two Curie temperature around 270 and 295 K indicating the presence of both  $\text{Mn}_5\text{Ge}_3$  and  $\text{Mn}_{11}\text{Ge}_8$  alloys. Since the deposition flux of Mn and Ge atoms are carefully kept in the  $\text{Mn}_5\text{Ge}_3$  stoichiometric ratio, the diffusion of the Ge atoms coming from the substrate is a governing factor explaining the difference since at 720 K the Ge flux of diffusion being higher, the local Ge concentration at the substrate/thin film interface leads to the preferential nucleation of  $\text{Mn}_{11}\text{Ge}_8$ .

#### 4.2 Sequence of the formation of the $\text{Mn}_5\text{Ge}_3$ and $\text{Mn}_{11}\text{Ge}_8$ phase in the SPE case

A 50 nm thick Mn film was deposited on a Ge(111) substrate, followed by an isochronic thermal annealing at  $5 \text{ K.min}^{-1}$  up to 860 K. The normalized and integrated intensities of the Mn(330),  $\text{Mn}_5\text{Ge}_3(002)$  and  $\text{Mn}_{11}\text{Ge}_8(223)$  diffraction peaks were recorded in real time during this annealing by in situ XRD measurements and shown in fig.4. Only one peak for each phase is plotted for clarity purpose.

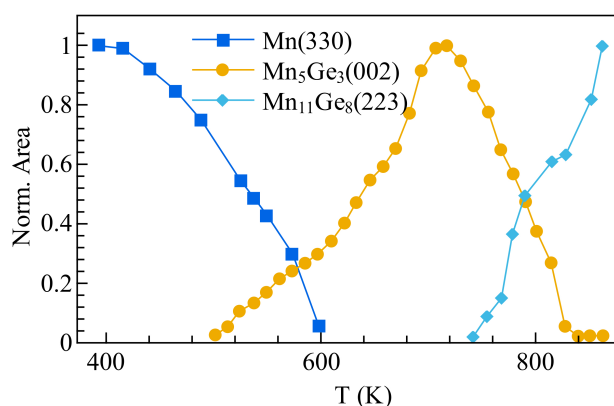


**Figure 4: Variations of integrated and normalized XRD peaks intensities versus annealing temperature in the case of the SPE growth of a  $\text{Mn}_5\text{Ge}_3$  thin film on a Ge(111) substrate.**

The evolution of the peaks intensities confirms the sequential phase formation.  $\text{Mn}_5\text{Ge}_3$  is the first phase to be nucleated at the sub-eutectic temperature of 500 K. These observation can be compared to the same experiment conducted on a Ge(001) substrate [33]. The shape of the variation of the  $\text{Mn}_5\text{Ge}_3(002)$  peak intensity exhibits a linear part from 500 K to 600 K. According to kinetic Monte Carlo simulation, this linear behavior may be explained by the prevalence of the nucleation process on other processes such as diffusion ones [21]. In solid phase reaction, intermixing at the interface is expected to take place at the concentration of the central eutectic point. At this concentration,  $\text{Mn}_5\text{Ge}_3$  is not the compound with the lowest effective heat of formation (fig.2) but is the closest congruent phase to the eutectic meaning the easiest phase to nucleate. The nucleation is the driving phenomenon in the formation of  $\text{Mn}_5\text{Ge}_3$  in the case of the SPE growth mode. Earlier works have studied the SPE growth of submonolayer to one monolayer thick Mn on Ge(111) [34]. The authors showed that the first formed Mn:Ge islands are composed of  $\text{Mn}_5\text{Ge}_3$  except for any other phase. As the temperature increases and reaches 740 K, the  $\text{Mn}_5\text{Ge}_3$  film starts to decompose and  $\text{Mn}_{11}\text{Ge}_8$  starts to form. The growth of a new phase occurs only it reduces the Gibbs free energy of the whole system. In the experimental range of temperature, diffusion processes are non-negligible. The finite size of the Mn-rich film compared to the Ge(111) substrate may induce an asymmetric Mn/Ge interdiffusion profile leading to a Ge enrichment at the interface and thus to  $\text{Mn}_{11}\text{Ge}_8$  becoming more favorable. In order to bring elements of discussion, we can mention that the Manganese diffusion in Ge(001) substrate is vacancy-mediated with a diffusivity close to the Ge self-diffusivity (the activation energy is around 2.37 eV) [35]. A low diffusion flux of Mn atoms into the Ge substrate is thus expected. On the contrary the epitaxial relationship between the  $\text{Mn}_5\text{Ge}_3$  thin films and Ge(111) leads to chains of octahedral interstitial sites along the  $\text{Mn}_5\text{Ge}_3[001]$  direction i.e. normal to the surface of the samples [36]. These chains may establish preferential diffusion path for the Ge atoms from the substrate to the thin film. Previous studies dealt with the sequence of phases

formation of a Mn film deposited on an amorphous Ge (a-Ge) layer [37]. The comparison between fig.4 and fig.2 of ref.[37] shows several differences. First the kinetics of the formation of  $Mn_5Ge_3$  is faster on an a-Ge layer than on a single crystalline Ge(111) substrate. The faster  $Mn_5Ge_3$  growth rate on a-Ge can be explained by the different diffusion paths used by Ge and Mn atoms in a polycrystalline  $Mn_5Ge_3$  layer grown on a-Ge where grain boundaries diffusion may take place and in a monocrystalline  $Mn_5Ge_3$  layer grown on Ge(111) where the lattice diffusion process is prevailing. Secondly the range of stability of the  $Mn_5Ge_3$  phase, before the nucleation of  $Mn_{11}Ge_8$ , is wider on a Ge(111) substrate ( $\Delta T = 320$  K versus 150 K on a-Ge). Together with the different diffusion paths, an epitaxial interface offering a low interface energy and few defects is expected to delay the germination of  $Mn_{11}Ge_8$  since the phase transformation (nucleation of a new phase) depends on the induced change in interface energy [29]. Thirdly the  $Mn_5Ge_3$  dissolution rate is slower in the case of a Ge(111) layer. As the  $Mn_{11}Ge_8$  layer is polycrystalline in both cases, the discrepancy in the rates rather comes from the crystalline quality of the  $Mn_5Ge_3$  films. We should note that surprisingly in ref [33], no other phase than  $Mn_5Ge_3$  is detected even at temperatures as high as 870 K.

#### 4.3 Thin films thickness and thermal stability of the $Mn_5Ge_3$ phase

Since the thickness of the  $Mn_5Ge_3$  thin films is a parameter influencing the magnetic properties of the film, the phase formation have been examined on two type of samples having tow different thicknesses [13]. The SPE growth was used to elaborate  $Mn_5Ge_3$  thin films on Ge(111) substrates with thicknesses of 20 and 70 nm. The annealing temperature for the SPE growth process was set at 720 K. The formed  $Mn_5Ge_3$  films were then post-annealed at two different temperatures  $T_{reheat}$  of 720 K and 970 K during 25 min. XRD measurements and  $M(T)$  curves were recorded on each post-annealed samples and are displayed on figure 5. The XRD measurements of the 20 nm films only clearly show the  $Mn_5Ge_3(002)$  peaks. The low amount of available matter makes it difficult to detect usable curves on the whole  $2\theta$  range. The  $M_{sat}(T)$  curves exhibit a similar law of decrease. However a small plateau on the curve corresponding to the 970 K re-heating can be seen between 100 and 160 K. This indicates the presence of a small quantity of the  $Mn_{11}Ge_8$  phase. Regarding the results for the 70 nm thick samples, the 2D-XRD maps (not shown here) exhibit partially ring-shaped patterns meaning the manganese germanide films are polycrystalline. The XRD spectrum of the 720 K re-heated film only exhibits the  $Mn_5Ge_3$  phase, while the  $Mn_{11}Ge_8$  phase is clearly identified in the 970 K post-annealed films. The  $M_{sat}(T)$  curves support the XRD observations. The 70 nm / 720 K curve reveals only the  $Mn_5Ge_3$  ferromagnetic signature while the 70 nm / 970 K is characterized by the  $Mn_{11}Ge_8$  anti-ferromagnetic transition at 150 K and lower Curie temperature coming from the sum of the ferromagnetic behaviour of the  $Mn_5Ge_3$  and  $Mn_{11}Ge_8$  phases. The combination of an

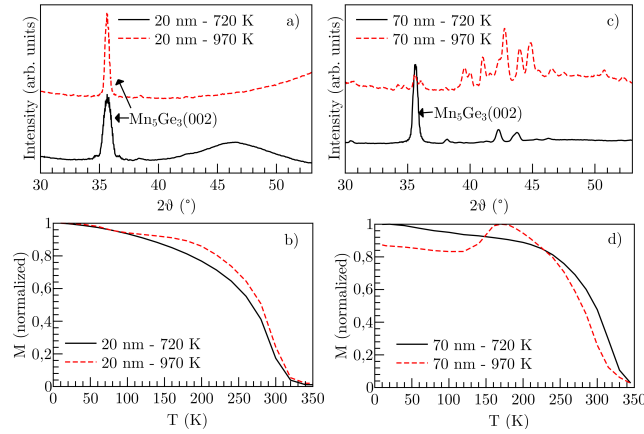


**Figure 5: XRD curves and normalized magnetization recorded on 20 (a-b) resp.) and 70 nm (c-d) resp.) thick  $Mn_5Ge_3$  films synthesized by the SPE growth mode and re-heated at 720 and 970 K in order to study the role of the thickness of the film on the thermal stability of the phase.**

increased thickness and post-annealings is detrimental to the crystallinity of the thin films and to the  $Mn_5Ge_3$  phase. A post-annealing tends to lead to the formation of the  $Mn_{11}Ge_8$  compound which agrees with a diffusion controlled phase formation. Indeed the thermal treatments entail a diffusive Ge flux coming from the substrate. Moreover, a previous work have shown that Mn diffusion along the [111] orientation of Ge is energetically unfavorable [38]. This asymmetric interdiffusion profile shifts the equilibrium towards  $Mn_{11}Ge_8$  favorable conditions. However the small proportion of the  $Mn_{11}Ge_8$  phase in the 20 nm / 970 K film cannot be explained considering only the diffusion phenomena. Two points may be contemplated.

First, the difference between the 20 nm and 70 nm series is the annealing time (cf. Fig.1 SPE step 2) needed to form the  $Mn_5Ge_3$  phase. This annealing time is longer for a sample thickness of 70 nm, as there are more Mn atoms to consume and transform into  $Mn_5Ge_3$ . Hence, the germination of the  $Mn_{11}Ge_8$  phase could have already occurred at the  $Mn_5Ge_3/Ge(111)$  interface for the thicker film during this first annealing step, the growth of the  $Mn_{11}Ge_8$  phase remaining only during the post-heating stage. Secondly the free energy  $\Delta G$  has a component related to the interfacial energy. As already mentioned,  $\gamma_{Mn_5Ge_3/Ge(111)}$  is low. According to the thickness and the resulting diffusion flux, the weighted importance of  $\gamma_{Mn_5Ge_3/Ge(111)}$  in  $\Delta G$  may lead to the swing of the thermodynamic equilibrium between maintaining a  $Mn_5Ge_3$  thin film on Ge(111) with the corresponding interface energy and forming the  $Mn_{11}Ge_8$  phase at the interface since  $\Delta H'_{Mn_{11}Ge_8} < \Delta H'_{Mn_5Ge_3}$  for Ge rich conditions.

## 5. Conclusion

The EHF model provides a suitable framework to explain the formation of the  $Mn_5Ge_3$  and  $Mn_{11}Ge_8$  phase in the manganese germanide thin films on Ge(111) substrates according to the used growth

270 methods. The model takes into account the different factors interplaying at the substrate/thin film interface. The key parameters of the growth process -substrate temperature, atoms fluxes- highlight the major role of the diffusion phenomena in the phase formation. The selection of the growth method -SPE, RDE or co-deposition- enables to control the phase formation of the manganese germanide thin films. In the case of the SPE, *In situ* X-ray diffraction shows a sequential formation  
275 of the phase.  $Mn_5Ge_3$  is the first formed phase, driven by the nucleation process. Then the diffusion phenomena shift the equilibrium, allowing the subsequent formation of  $Mn_{11}Ge_8$  by consuming  $Mn_5Ge_3$ . A comparison with a previous work dealing with the SPE growth on an a-Ge layer and the study of the effect of the film thickness show the role of the interface on the stability of the  $Mn_5Ge_3$  phase. The epitaxy of  $Mn_5Ge_3$  on Ge(111) expands the range of the thermal stability of this phase  
280 which is a key point for a potential use of  $Mn_5Ge_3$  as a ferromagnetic metallic contact for spin injection.

### Acknowledgment

Part of this work was done with the help of the PICS n°200835 TRANPOLSPIN  
285 (CINaM-CNRS/AIST) project.

### References

- [1] E.Y. Vedmedenko, R.K. Kawakami, D.D. Sheka, P. Gambardella, A. Kirilyuk, A. Hirohata, C. Binek, O. Chubykalo-Fesenko, S. Sanvito, B.J. Kirby, J. Grollier, K. Everschor-Sitte, T. Kampfrath, C.Y. You, A. Berger, The 2020 magnetism roadmap, *J. Phys. D: Appl. Phys.* 53 (2020). <https://doi.org/10.1088/1361-6463/ab9d98>.  
290
- [2] U. Gösele, K.N. Tu, Growth kinetics of planar binary diffusion couples: “Thin-film case” versus “bulk cases,” *J. Appl. Phys.* 53 (1982) 3252–3260. <https://doi.org/10.1063/1.331028>.
- [3] S. Gaudet, C. Detavernier, A.J. Kellock, P. Desjardins, C. Lavoie, Thin film reaction of transition metals with germanium, *J. Vac. Sci. Technol. A Vacuum, Surfaces, Film.* 24 (2006) 474–485. <https://doi.org/10.1116/1.2191861>.  
295
- [4] C.. Churms, C.. Comrie, R.. Nemutudi, Study of Pd/Ge interaction in a lateral diffusion couple by microbeam Rutherford backscattering spectrometry, *Nucl. Instruments Methods Phys. Res. Sect. B Beam Interact. with Mater. Atoms.* 158 (1999) 713–716. [https://doi.org/10.1016/S0168-583X\(99\)00307-9](https://doi.org/10.1016/S0168-583X(99)00307-9).  
300
- [5] C. Zeng, S.C. Erwin, L.C. Feldman, A.P. Li, R. Jin, Y. Song, J.R. Thompson, H.H. Weitering, Epitaxial ferromagnetic  $Mn_5Ge_3$  on Ge(111), *Appl. Phys. Lett.* 83 (2003) 5002–5004. <https://doi.org/10.1063/1.1633684>.
- [6] M. Gajdzik, C. Sürgers, M.T. Kelemen, H. v. Löhneysen, Strongly enhanced Curie temperature in carbon-doped  $Mn_5Ge_3$  films, *J. Magn. Mater.* 221 (2000) 248–254. [https://doi.org/DOI: 10.1016/S0304-8853\(00\)00494-7](https://doi.org/DOI:10.1016/S0304-8853(00)00494-7).  
305

- [7] Y. Tawara, K. Sato, On the magnetic anisotropy of single crystal of Mn<sub>5</sub>Ge<sub>3</sub>, *J. Phys. Soc. Japan.* 18 (1963) 773–777. <https://doi.org/10.1143/JPSJ.18.773>.
- [8] A. Spiesser, F. Viot, L.-A. Michez, R. Hayn, S. Bertaina, L. Favre, M. Petit, V. Le Thanh, Magnetic anisotropy in epitaxial Mn<sub>5</sub>Ge<sub>3</sub> films, *Phys. Rev. B.* 86 (2012) 035211. <https://doi.org/10.1103/PhysRevB.86.035211>.
- [9] A. Spiesser, H. Saito, R. Jansen, S. Yuasa, K. Ando, Large spin accumulation voltages in epitaxial Mn<sub>5</sub>Ge<sub>3</sub> contacts on Ge without an oxide tunnel barrier, *Phys. Rev. B.* 90 (2014) 1–9. <https://doi.org/10.1103/PhysRevB.90.205213>.
- [10] M. Petit, R. Hayakawa, Y. Wakayama, V. Le Thanh, L. Michez, Mn<sub>5</sub>Ge<sub>3</sub>C<sub>0.6</sub>/Ge(111) Schottky contacts tuned by an n-type ultra-shallow doping layer, *J. Phys. D. Appl. Phys.* 49 (2016) 355101. <https://doi.org/10.1088/0022-3727/49/35/355101>.
- [11] M. Petit, L. Michez, C.-E. Dutoit, S. Bertaina, V.O. Dolocan, V. Heresanu, M. Stoffel, V. Le Thanh, Very low-temperature epitaxial growth of Mn<sub>5</sub>Ge<sub>3</sub> and Mn<sub>5</sub>Ge<sub>3</sub>C<sub>0.2</sub> films on Ge(111) using molecular beam epitaxy, *Thin Solid Films.* 589 (2015) 427–432. <https://doi.org/10.1016/j.tsf.2015.05.068>.
- [12] S.F. Olive-Mendez, A. Spiesser, L.A. Michez, V. Le Thanh, A. Glachant, J. Derrien, T. Devillers, A. Barski, M. Jamet, Epitaxial growth of Mn<sub>5</sub>Ge<sub>3</sub>/Ge(111) heterostructures for spin injection, *Thin Solid Films.* 517 (2008) 191–196. <https://doi.org/DOI:10.1016/j.tsf.2008.08.090>.
- [13] L.-A. Michez, A. Spiesser, M. Petit, S. Bertaina, J. Jacquot, D. Dufeu, C. Coudreau, M. Jamet, V. Le Thanh, Magnetic reversal in Mn<sub>5</sub>Ge<sub>3</sub> thin films: an extensive study, *J. Phys. Condens. Matter.* 27 (2015) 266001. <https://doi.org/10.1088/0953-8984/27/26/266001>.
- [14] N. Yamada, K. Maeda, Y. Usami, T. Ohoyama, Magnetic properties of intermetallic compound Mn<sub>11</sub>Ge<sub>8</sub>, *J. Phys. Soc. Japan.* 55 (1986) 3721–3724. <https://doi.org/http://doi.org/10.1143/JPSJ.55.3721>.
- [15] E. Arras, D. Caliste, T. Deutsch, F. Lançon, P. Pochet, Phase diagram, structure, and magnetic properties of the Ge-Mn system: A first-principles study, *Phys. Rev. B.* 83 (2011) 1–12. <https://doi.org/10.1103/PhysRevB.83.174103>.
- [16] A. Vantomme, S. Degroote, J. Dekoster, G. Langouche, R. Pretorius, Concentration-controlled phase selection of silicide formation during reactive deposition, *Appl. Phys. Lett.* 74 (1999) 3137–3139. <https://doi.org/10.1063/1.124090>.
- [17] R.M. Walser, R.W. Bené, First phase nucleation in silicon-transition-metal planar interfaces, *Appl. Phys. Lett.* 28 (1976) 624–625. <https://doi.org/10.1063/1.88590>.
- [18] G. Ottaviani, Metallurgical aspects of the formation of silicides, *Thin Solid Films.* 140 (1986) 3–22. [https://doi.org/10.1016/0040-6090\(86\)90154-9](https://doi.org/10.1016/0040-6090(86)90154-9).
- [19] R. Pretorius, A.M. Vredenberg, F.W. Saris, R. De Reus, Prediction of phase formation sequence and phase stability in binary metal-aluminum thin-film systems using the effective heat of formation rule, *J. Appl. Phys.* 70 (1991) 3636–3646. <https://doi.org/10.1063/1.349211>.

- [20] B. De Schutter, K. De Keyser, C. Lavoie, C. Detavernier, Texture in thin film silicides and germanides: A review, *Appl. Phys. Rev.* 3 (2016). <https://doi.org/10.1063/1.4960122>.
- [21] A. Portavoce, G. Tréglia, Theoretical investigation of the influence of reaction and diffusion kinetics upon thin-film reactive diffusion, *Phys. Rev. B.* 85 (2012) 1–13.  
350 <https://doi.org/10.1103/PhysRevB.85.224101>.
- [22] R.W. Bené, A kinetic model for solid-state silicide nucleation, *J. Appl. Phys.* 61 (1987) 1826–1833. <https://doi.org/10.1063/1.338025>.
- [23] A.B. Gokhale, R. Abbaschian, The Ge-Mn (Germanium-Manganese) System, *J. Phase Equilibria.* 11 (1990) 460–468. <https://doi.org/10.1007/BF02898261>.
- 355 [24] R. Pretorius, Phase sequence of silicide formation at metal-silicon interfaces, *Vacuum.* 41 (1990) 1038–1042. [https://doi.org/10.1016/0042-207X\(90\)93854-C](https://doi.org/10.1016/0042-207X(90)93854-C).
- [25] R. Pretorius, T.K. Marais, C.C. Theron, Thin film compound phase formation sequence: An effective heat of formation model, *Mater. Sci. Reports.* 10 (1993) 1–83.  
[https://doi.org/10.1016/0920-2307\(93\)90003-W](https://doi.org/10.1016/0920-2307(93)90003-W).
- 360 [26] R. Pretorius, C.C. Theron, A. Vantomme, J.W. Mayer, Compound phase formation in thin film structures, *Crit. Rev. Solid State Mater. Sci.* 24 (1999) 1–62.  
<https://doi.org/10.1080/10408439991329161>.
- [27] A. Berche, J.C. Tedenac, P. Jund, Thermodynamic modeling of the germanium-manganese system, *Intermetallics.* 47 (2014) 23–30. <https://doi.org/10.1016/j.intermet.2013.12.009>.
- 365 [28] M. Ronay, Reinvestigation of first phase nucleation in planar metal-Si reaction couples, *Appl. Phys. Lett.* 42 (1983) 577–579. <https://doi.org/10.1063/1.94007>.
- [29] F.M. d’Heurle, P. Gas, Kinetics of formation of silicides: A review, *J. Mater. Res.* 1 (1986) 205–221. <https://doi.org/10.1557/JMR.1986.0205>.
- [30] P. Gas, F.M. d’Heurle, Formation of silicide thin films by solid state reaction, *Appl. Surf. Sci.* 73 (1993) 153–161. [https://doi.org/10.1016/0169-4332\(93\)90160-D](https://doi.org/10.1016/0169-4332(93)90160-D).
- 370 [31] A. Portavoce, G. Tréglia, Physical origin of thickness-controlled sequential phase formation during reactive diffusion: Atomistic modeling, *Phys. Rev. B.* 82 (2010) 1–12.  
<https://doi.org/10.1103/PhysRevB.82.205431>.
- [32] E. Arras, Étude théorique de la structure et de la stabilité des alliages GeMn dans le cadre de la spintronique. Un prototype de semiconducteur magnétique confronté aux résultats expérimentaux., PhD thesis, Université Joseph-Fourier - Grenoble I, 2010.
- 375 [33] M. Wittmer, M.-A. Nicolet, J.W. Mayer, The first phase to nucleate in planar transition metal-germanium interfaces, *Thin Solid Films.* 42 (1977) 51–59. [https://doi.org/DOI:10.1016/0040-6090\(77\)90077-3](https://doi.org/DOI:10.1016/0040-6090(77)90077-3).
- 380 [34] C. Zeng, W. Zhu, S.C. Erwin, Z. Zhang, H.H. Weitering, Zeng, C., Zhu, W., Erwin, S. C., Z. Zhang, Zhenyu, Weitering, Hanno H., Initial stages of Mn adsorption on Ge(111), *Phys. Rev. B.* 70 (2004) 2–9. <https://doi.org/10.1103/PhysRevB.70.205340>.

- 385 [35] A. Portavoce, O. Abbes, Y. Rudzevich, L. Chow, V. Le Thanh, C. Girardeaux, Manganese diffusion in monocrystalline germanium, *Scr. Mater.* 67 (2012) 269–272. <https://doi.org/10.1016/j.scriptamat.2012.04.038>.
- [36] P. De Padova, J.M. Mariot, L. Favre, I. Berbezier, B. Olivieri, P. Perfetti, C. Quaresima, C. Ottaviani, a. Taleb-Ibrahimi, P. Le Fèvre, F. Bertran, O. Heckmann, M.C. Richter, W. Ndiaye, F. D’Orazio, F. Lucari, C.M. Cacho, K. Hricovini, Mn<sub>5</sub>Ge<sub>3</sub> films grown on Ge(1 1 1)-c(2 × 8), *Surf. Sci.* 605 (2011) 638–643. <https://doi.org/10.1016/j.susc.2011.01.002>.
- 390 [37] O. Abbes, A. Portavoce, V. Le Thanh, C. Girardeaux, L. Michez, Phase formation during Mn thin film reaction with Ge: Self-aligned germanide process for spintronics, *Appl. Phys. Lett.* 103 (2013) 172405. <https://doi.org/10.1063/1.4827100>.
- 395 [38] W. Zhu, H.H. Weitering, E. Wang, E. Kaxiras, Z. Zhang, Contrasting Growth Modes of Mn on Ge(100) and Ge(111) Surfaces: Subsurface Segregation versus Intermixing, *Phys. Rev. Lett.* 93 (2004) 91–94. <https://doi.org/10.1103/PhysRevLett.93.126102>.